

Photodegradation of Atmospheric Chromophores: Changes in Oxidation State and Photochemical Reactivity

Zhen Mu^a, Qingcai Chen^{a*}, Lixin Zhang^a, Dongjie Guan^a and Hao Li^a

^a *School of Environmental Science and Engineering, Shaanxi University of Science and Technology, Xi'an 710021, China*

*Corresponding authors:

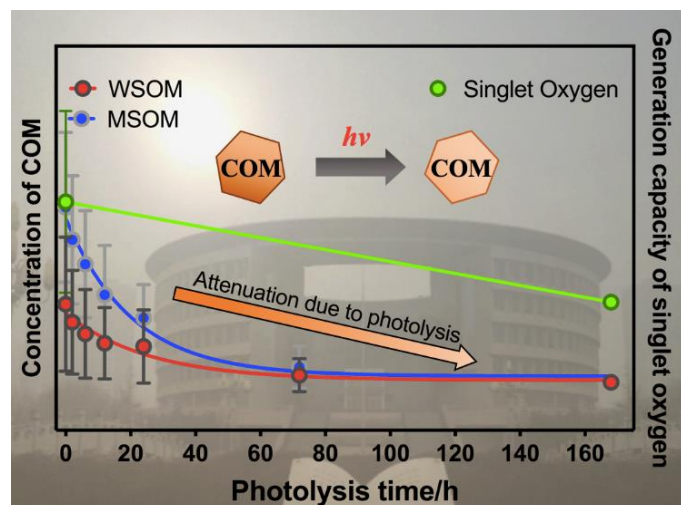
School of Environmental Science and Engineering, Shaanxi University of Science and Technology, Weiyang District, Xi'an, Shaanxi, 710021, China.

*(Q. C.) Phone: (+86) 0029-86132765; e-mail: chenqingcai@sust.edu.cn;

1 **Abstract:** Atmospheric chromophoric organic matter (COM) plays a fundamental role in
2 photochemistry and aerosol aging. However, the effects of photodegradation on chemical
3 components and photochemical reactivity of COM are remain unresolved. Here, we report the
4 potential impacts of photodegradation on carbon content, optical property, fluorophore component,
5 and photochemical reactivity of organic aerosols. After 7 days of photodegradation, fluorescent
6 intensity and absorption coefficient of water-soluble and methanol-soluble COM decrease by 71.4%
7 and 32.0% on average, respectively. Low oxidation humic-like substance (HULIS) is converted into
8 high oxidation HULIS due to photooxidation, the result suggests that the chromophore composition
9 has changed as well as the degree of aerosol aging. COM photodegradation has a significant impact
10 on photochemical reactivity. The generation rate constants of triplet state COM (${}^3\text{COM}^*$) decrease
11 slightly in ambient particulate matter (ambient PM) but increase in primary organic aerosol (POA)
12 following photodegradation. The results highlight that the opposite effect of photodegradation on
13 photochemical reactivity in POA and ambient PM. The ability of COM generating singlet oxygen
14 (${}^1\text{O}_2$) decreases obviously, which could be attributed to photodegradation of chromophoric
15 precursors of ${}^1\text{O}_2$. The combination of optical property, chemical component, and reactive oxygen
16 species have an important impact on the atmosphere quality. The new insights on photodegradation
17 of COM in aerosol reinforce the importance of studying DOM related with the photochemistry and
18 aerosol aging.

19 **Key word:** atmospheric chromophore; photodegradation; EEMs; triplet state; reactive oxygen
20 species.

21 **TOC:**



22

23 **1. Introduction**

24 Atmospheric chromophoric organic matter (COM) mainly originates from biomass
25 combustion emission and secondary organic aerosol (SOA) (Andreae & Gelencser, 2006;
26 Budisulistiorini et al., 2017; Gruber & Rudich, 2005; Zappoli et al., 1999). Because of the significant
27 absorption for short-wave radiation (Wavelength range from near-ultraviolet light to visible light)
28 (Rosario-Ortiz and Canonica, 2016; Cheng et al., 2016), COM may undergo photochemical
29 processing and have a significant impact on atmospheric components and quality (Zhao et al., 2013;
30 Jo et al., 2016). Therefore, simulation and evaluation of COM photochemistry are necessary for
31 understanding aerosol aging.

32 As photosensitive substances, the optical properties and components of COM change
33 significantly under solar irradiation (Alkinson et al., 2016; Carlton et al., 2007; Lee et al., 2013;
34 Murphy et al., 2013). On the one hand, optical properties change significantly that due to COM is
35 photo-bleaching in aerosol. Zhong and Jang (2014) reported that mass absorption coefficients (MAC)
36 decreased by 41% on average because wood-burning organic matter (OM) was bleaching, such as
37 conjugated aromatic rings and phenols, and hydroxylated aromatic phenols; Lee et al. (2014) also
38 reported that the MAC of secondary organic aerosol (SOA) continued to decrease in the UV-Vis
39 spectral. On the other hand, photodegradation has a significant effect on the chemical components
40 of COM. COM can be decomposed into small molecules after photodegradation and the
41 photodegraded COM may have lower volatility and higher oxidation degree (Grieshop et al., 2009).
42 COM could also be generated through the photochemical processes, which could be attributed to
43 the formation of SOA. For example, oligomeric COM could be generated by a mixture of anthracene
44 and naphthalene suspensions through self-oxidation under solar irradiation and photo-oxidation of
45 aromatic isoprene oxides were an important source of high molecular weight COM (Altieri et al.,
46 2006; Altieri et al., 2008; Haynes et al., 2019; Holmes and Petrucci, 2006; Perri et al., 2009). SOA
47 may have a more significant light absorption than primary organic aerosol (POA) in the short-
48 wavelength visible and near-UV region (Zhong & Jang, 2014; Saleh et al., 2013; Harrison et al.,
49 2020). As a result, photodegradation plays an important role in the components and properties of
50 COM and thereby change photochemical activity. There are limited studies that comprehensively
51 exploring the characteristics of photodegradation of COM in aerosol.

52 Photochemical process of COM largely determines the aerosol aging (Mang et al., 2008). On
53 the one hand, COM is often used as reactant in photochemical processes in aerosol. For example,
54 COM could be oxidized by hydroxyl radicals ($\bullet\text{OH}$). The formation of polyols can be attributed to
55 photooxidation of isoprene, which could be initiated by $\bullet\text{OH}$ (Claeys et al., 2004; Zhao et al., 2015).
56 Humic-like substance (HULIS) with complex functional groups has significant contribution to
57 photochemistry (George et al., 2015; Nebbioso & Piccolo, 2013; Wenk et al., 2013). On the other
58 hand, COM also participates in atmospheric photochemistry process indirectly through generating
59 reactive intermediates, energy transferring, and involving electron. Upon light exposure, high-
60 energy singlet state COM (${}^1\text{COM}^*$) could be excited. ${}^1\text{COM}^*$ deactivates by emitting photon

61 (fluorescence) and intersystem crossing (triplet state (${}^3\text{COM}^*$) generation). ${}^3\text{COM}^*$ not only can
62 produce photochemical reaction directly, but also can generate reactive oxygen species (ROS), such
63 as singlet oxygen (${}^1\text{O}_2$), super oxide (O_2^-), and $\cdot\text{OH}$, which indicates that ${}^3\text{COM}^*$ plays a critical
64 role in ROS formation and pollutant attenuation (Paul Hansard et al., 2010; Szymczak & Waite,
65 1988; Zhang et al., 2014; Rosario-Ortiz and Canonica, 2016; Sharpless, 2012; Haag and Gassman,
66 1984; Zhou et al., 2019). A lot of COM, such as aromatic ketones (Canonica et al., 2006; Marciniak
67 et al., 1993), benzophenone (Encinas et al., 1985), and phenanthrene (Wawzonek & Laitinen, 1942),
68 have been identified as the precursors of ${}^3\text{COM}^*$. Chemical probes, such as 2,4,6-trimethylphenol
69 (TMP) and sorbic acid (SA), are applicable to evaluate the productivity of ${}^3\text{COM}^*$ (Zhou et al.,
70 2019; Moor et al., 2019; Chen et al., 2021). Compared with ${}^1\text{COM}^*$, the characteristics of ${}^3\text{COM}^*$
71 are lower formation rate (15~100 times slower than ${}^1\text{COM}^*$), lower quenching rate (20000 times
72 lower than ${}^1\text{COM}^*$), and higher steady-state concentration (200~1300 times higher than ${}^1\text{COM}^*$)
73 (McNeil et al., 2016). Therefore, the reaction rate constant of ${}^3\text{COM}^*$ is used in evaluating the
74 photochemical reactivity. Considering the potential effect of ROS on aerosol aging and atmospheric
75 quality, it is necessary to clarify the path and mechanism.

76 COM photochemistry may dominate the chemical composition and the aerosol aging process.
77 In order to illustrate the properties of COM photodegradation and the effect of COM
78 photodegradation on aerosol aging, we simulate the process of COM photodegradation and COM
79 generating ROS in the laboratory. The objectives of the study are (1) to clarify the variation
80 characteristics of carbon content during the COM photodegradation process, (2) to explore the
81 effects of photodegradation on fluorophores and optical properties in water-soluble and methanol-
82 soluble COM, and (3) to investigate the effect of COM photodegradation on photochemical
83 reactivity (photochemical reactivity is characterized by the generation capacity of triplet state and
84 singlet oxygen).

85 **2. Experimental Section**

86 *2.1 Sample Collection*

87 A total of 16 samples were collected (The details of the samples are shown in **Table S1** of SI).
88 The ambient PM samples were collected in Shaanxi University of Science and Technology, Xi'an,
89 Shaanxi Province (N34°22'35.07", E108°58'34.58"; the altitude of sampling location was about 30
90 m). The ambient PM samples were collected on quartz fiber filter (Pall life sciences, America) by
91 an intelligent large-flow sampler (Xintuo XT-1025, China) with a sampling time of 23 h 30 min and
92 a sampling flow rate of 1000 L/min. The ambient PM samples were stored in the refrigerator at -
93 20 °C prior to use.

94 The POA samples were collected through a combustion chamber. Straw and coal burning were
95 the main way of heating and cooking in the rural areas in China. Therefore, wheat straw-, corn
96 straw-, rice straw-, and wood-burning samples were collected (Schematic diagram of combustion
97 chamber is shown in **Figure S1**). The POA samples were stored in the refrigerator at -20 °C prior
98 to use.

99 2.2 Photodegradation experiment

100 A quartz reactor was designed for photodegradation experiment (Schematic diagrams of the
101 photochemical devices are shown in **Figure S2**; The detail of the reactor has been described in
102 previous study (Chen et al., 2021)). The photodegradation times were 0 h, 2 h, 6 h, 12 h, 24 h, 3 d
103 and 7 d and a series of photodegraded samples were collected.

104 2.3 Carbon content measurement

105 The original and photodegraded samples were ultrasonic extracted with ultrapure water (>18.2
106 MΩ•cm, Hitech, China) and filtered through a 0.45 μm filter (Jinteng, China) to obtain the water-
107 soluble organic matter (WSOM). After water extraction, residual organic matter were further
108 extracted with methanol (HPLC Grade, Fisher Chemical, America) and filtered through a 0.45 μm
109 filter to obtain methanol-soluble organic matter (MSOM). The blank samples were also extracted
110 with the same method.

111 The measurement method of carbon content has been described previously (Mu et al., 2019).
112 Briefly, 100 μL extract was injected on the baked quartz filter. Then, the wet filter was dried out by
113 a rotary evaporator and the dried filter was analyzed by the OC/EC online analyzer (Model 4, Sunset,
114 America) with the approach of NIOSH 870 protocol (Karanasiou et al., 2015). Organic carbon (OC)
115 was measured in the absence of oxygen. An oven in the instrument was filled with helium and
116 temperature was risen in a gradient style. Different temperatures are needed for particular analysis
117 phases (OC1-310 °C, OC2-472 °C, OC3-615, OC4-850 °C). Element carbon (EC) was measured in
118 the present of oxygen. The oven in the instrument was filled with helium-oxygen gas mixture (He/O₂
119 = 9/1). Different temperatures were also needed for particular analysis phases (EC1-550 °C, EC2-
120 625 °C, EC3-700°C, EC4-775 °C, EC5-850 °C, EC6-870 °C). The products in the heating process
121 were further oxidized to CO₂. The carbon content was obtained through the measurement of CO₂.
122 Six parallel samples were analyzed and the uncertainty of the method was <3.7% (one standard
123 deviation).

124 2.4 Optical analysis

125 The light absorption and EEM spectra of WSOM and MSOM were measured by an Aqualog
126 fluorescence spectrophotometer (Horiba Scientific, America). The range of excitation wavelength
127 was 200-600 nm with an interval of 5 nm. The range of emission wavelength was 250-800 nm. The
128 integration time was 0.5 s. The absorption spectra was also recorded in the wavelength range of
129 200-600 nm. Water and methanol blank samples were measured using the same method and the
130 blank value was subtracted from the sample value. The extracts were diluted to reduce internal
131 filtration effect (The concentrations and dilution factors are shown in **Table S2** of SI).

132 The EEM data was analyzed by parallel factor analysis model (PARAFAC) to identify
133 fluorophores (The model referred to the previous papers (Murphy et al., 2013; Chen et al., 2016a;
134 Chen et al., 2016b)). WSOM and MSOM (111 samples) were combined in the dataset to create the
135 PARAFAC model. According to the EEM characteristics and the residual error variation trend of the

136 2-7 component PARAFAC models, 4 fluorescent components were identified (Error analysis of the
137 models is shown in **Figure S4** of SI).

138 *2.5 Triplet state generation experiment*

139 As short-lived reactive intermediates, ${}^3\text{COM}^*$ has an important impact on photochemical
140 process in atmospheric environment (Kaur et al., 2018). Therefore, changes in ${}^3\text{COM}^*$ generation
141 ability before and after photodegradation were studied. The samples with the photodegradation time
142 of 0 and 7 d were defined as the original and photolyzed samples, respectively. Only WSOM of
143 original and photolyzed samples was used in the triplet state generation experiment. A capsule
144 (**Figure S2(c)**) was designed for this experiment. TMP was used as the capturing agent for the
145 ${}^3\text{COM}^*$. 60 μL of WSOM extract (Carbon content is shown in **Table S3**) and 60 μL of TMP solution
146 ($c_{\text{TMP}} = 20 \mu\text{M}$, Aladdin, China) were mixed in the capsule. The capsule was placed in the reactor
147 (**Figure S2(a)**). The times of optical excitation were 0, 5, 10, 15, 30, 45, 60 and 90 min, respectively.
148 Then 90 μL mixed solution was taken out from the capsule at different time points and 30 μL of
149 phenol solution ($c_{\text{phenol}} = 50 \mu\text{M}$, Aladdin, China) was added into the mixed solution (Phenol
150 solution was used as the internal standard substance for TMP quantification).

151 TMP was measured by liquid chromatography (LC). The method was as follows: C18 column
152 (Xuanmei, China); mobile phase: acetonitrile/water = 1/1 (v/v); flow rate: 1 mL/min; UV detector:
153 detection wavelength 210 nm. The retention time was 14.5 min. Kaur & Anastasio (2018) and
154 Richards-Henderson et al. (2015) have reported that TMP consumption conformed to first-order
155 kinetics. The curvy fitting was performed by exponential function among the TMP concentration
156 ($c_{\text{TMP}}/\mu\text{M}$), the optical excitation time (t/min) and triplet state generation rate constant ($k_{\text{TMP}}/\text{min}^{-1}$):

$$c_{\text{TMP}} = a \cdot e^{-t \times k_{\text{TMP}}} \quad (1)$$

158 *2.6 Singlet oxygen generation experiment*

159 The effect of COM photodegradation on singlet oxygen was studied. A capsule (**Figure S2(b)**)
160 was designed for ${}^1\text{O}_2$ generation experiment. Only WSOM of original and photolyzed was used in
161 the singlet oxygen generation experiment. 4-Hydroxy-2, 2, 6, 6-tetramethylpiperidine (TEMP,
162 $c_{\text{TEMP}}=240 \text{ mM}$, Aladdin, China) was used as the capturing agent for ${}^1\text{O}_2$ and ${}^1\text{O}_2$ was measured by
163 EPR spectrometer (MS5000, Freiberg, Germany). SA ($c_{\text{SA}}=133.3 \mu\text{M}$, Aladdin, China) was used as
164 quenching agent for ${}^3\text{COM}^*$. The method was as follows: (1) ${}^1\text{O}_2$ was measured before optical
165 excitation. 40 μL WSOM, 40 μL TEMP, and 40 μL ultra-pure water were mixed in the capsule
166 (**Figure S2(b)**). Then, 50 μL of the mixed solution was taken out by capillary for EPR analysis; (2)
167 ${}^1\text{O}_2$ was measured without optical excitation after 60 min. 40 μL WSOM, 40 μL TEMP and 40 μL
168 ultra-pure water were mixed in the capsule. The capsule was placed in the reactor for 60 min without
169 illumination. Then 50 μL mixed solution was taken out by capillary for EPR analysis; (3) ${}^1\text{O}_2$ was
170 measured after 60 min of optical excitation. 40 μL WSOM, 40 μL TEMP and 40 μL ultra-pure
171 water were mixed in the capsule. The capsule was illuminated in the reactor for 60 min. 50 μL
172 mixed solution was taken out by capillary for EPR analysis; (4) ${}^3\text{COM}^*$ was quenched and ${}^1\text{O}_2$ was
173 measured after 60 min of optical excitation. 40 μL WSOM, 40 μL TEMP and 40 μL SA solution

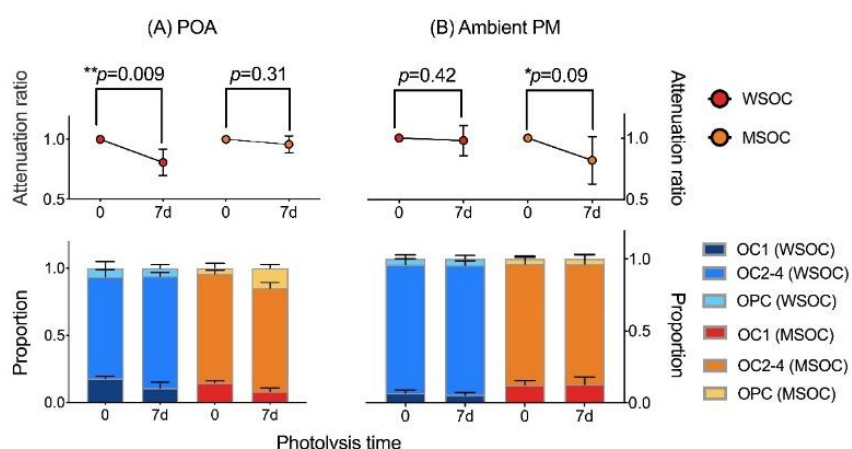
174 were mixed in capsule. The mixed sample was illuminated in the reactor for 60 min, then 50 μ L
175 mixed solution was taken out by capillary for EPR analysis.

176 3. Results and discussion

177 3.1 Effect of COM photodegradation on carbon content

178 **Figure 1** describes the changes in carbon content before and after COM photodegradation. In
179 POA (**Figure 1(A)**), water-soluble and methanol-soluble organic carbon (WSOC and MSOC)
180 decrease by 22.1% and 3.5%, respectively. The results suggest that WSOC tend to be photodegraded
181 in POA. In WSOC, the proportion of OC1 (OC1 and OC2-4 are the different stage in the process of
182 thermal-optical analysis) decreases significantly, which is the main loss of OC. OC1 are
183 characterized by small molecular weight and highly volatile (Karanasiou et al., 2015) and OC with
184 these characteristics tend to be photodegraded. In MSOC, there is a process of OC1 translating into
185 pyrolysis carbon (OPC). The proportion of OPC in MSOC shows an increasing trend (an average
186 increase of 2.4 times). Pyrolysis carbon is identified as oxygen-containing organic substance. Thus,
187 the increasing oxygen-containing organic matter may be due to the photo-inducing oxidation
188 reaction.

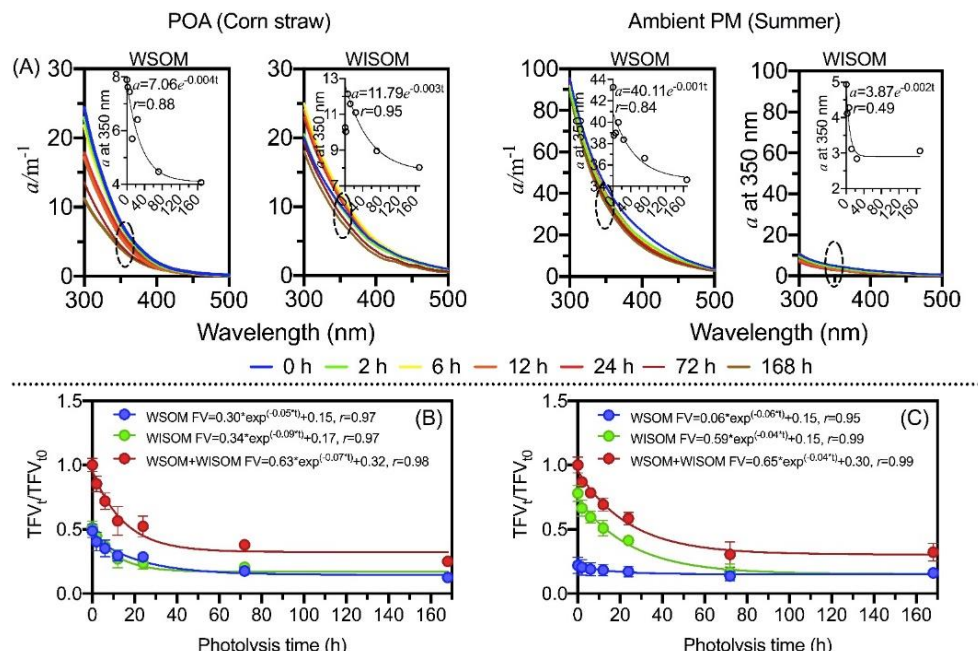
189 POA is fresh and ambient PM has undergone long-term aerosol aging. In ambient PM (**Figure**
190 **1(B)**), WSOC is nearly unchanged and MSOC decreases by 18.2%, which is in contrast to POA.
191 The results reflect that OM has been photodegraded adequately following the photodegradation and
192 mineralization process in WSOM of ambient PM. However, MSOC with high molecular weight
193 could not be photodegraded adequately and thereby continue to be photodegraded in laboratory.
194 The proportions of OC1, OC2-4, and OPC are relatively stable in ambient PM, which indicates that
195 the decreasing proportions in the different stages are similar and the tendency is also in contrast to
196 POA. The result reflects that different molecular weight OM may have the similar abilities of
197 photodegradation in ambient PM. The proportion of different molecular weight OM is nearly
198 unchanged following the photodegradation in ambient PM.



199
200 **Figure 1** Changes in carbon content before and after photodegradation. The *p*-value is the probability that two sets
201 of data have the same level (two-tailed test). * and ** are the significant difference at the 0.1 and 0.01 levels,
202 respectively.

203 3.2 Effect of COM photodegradation on optical properties

204 As shown in **Figure 2**, both absorption coefficient and total fluorescence volume (TFV, RU-
 205 nm²/m³) significantly decrease following photodegradation, which suggests that COM is photo-
 206 bleaching (Aiona et al., 2018; Duarte et al., 2005; Liu et al., 2016). The attenuations of fluorescence
 207 intensity and absorption coefficient are fitted to first-order decay. The absorption coefficient
 208 decreases by 32.0% and TFV decreases by 71.4% on average. However, as shown in **Figure 3**,
 209 fluorescence intensities increase and decrease in different regions of EEMs (Aiona et al., 2018;
 210 Timko et al., 2015).



211 **Figure 2** Changes in absorption coefficient and fluorescence volume during the photodegradation process. (A)
 212 Absorption coefficient. The scatter plot is absorption coefficient at 350 nm. (B) and (C) the attenuation curve of
 213 fluorescence volume in POA (except for the wood sample) and ambient PM, respectively.
 214

215 In POA (**Figure 2(B)**), TFV decreases by 74.8% on average and the exponential curve method
 216 was used to analysis the attenuation of fluorescence intensity. The attenuation of TFV are significant
 217 similarities between WSOM and MSOM. However, wood-burning samples are distinct from other
 218 POA samples, TFV of wood-burning COM only decreases by 9.0% and fluorescence volume of
 219 MSOM of wood-burning samples remain almost unchanged (**Figure S7**). There are two main
 220 reasons. On the one hand, methanol-soluble secondary OM is generated slightly in wood-burning
 221 samples (Zhong & Jang, 2014). On the other hand, methanol-soluble wood-burning COM is
 222 difficultly photodegraded. In addition, fluorophores photodegradation also depends on the
 223 photochemical environment, such as solution pH (Aiona et al., 2018), salinity (Xu et al., 2020), and

224 temperature (Yang et al., 2021). Therefore, we suppose that photodegradation of wood-burning
225 COM may largely depend on photodegradation environment.

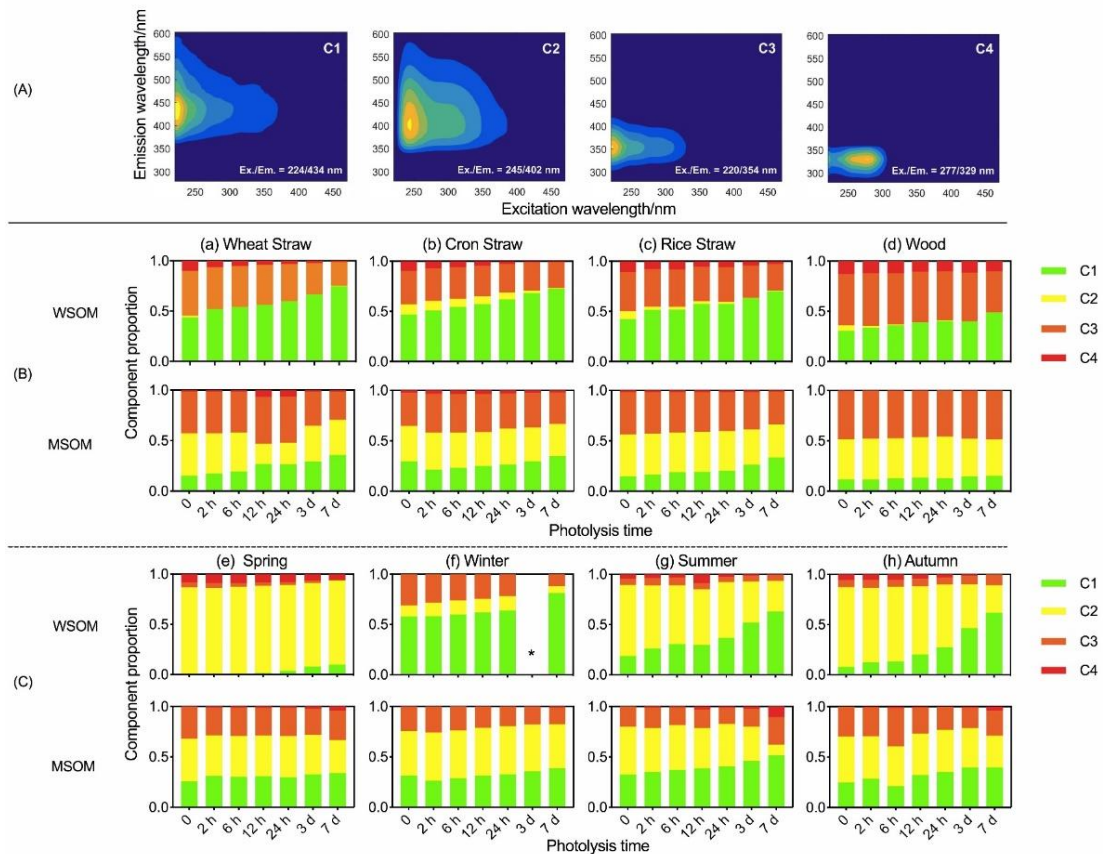
226 The attenuation rate constant of TFV in ambient PM ($k = 0.04 \text{ h}^{-1}$) is lower than that in POA
227 ($k = 0.07 \text{ h}^{-1}$). In ambient PM, TFV of MSOM decreases by 79.4% but WSOM decreases by 26.7%
228 (**Figure 2(C)**). The attenuation of TFV and carbon content is identical with each other. The results
229 suggest that MSOM has greater ability to be photodegraded than WSOM in ambient PM. It is worth
230 noting that 72 h could be considered as the end point of aerosol photo-aging because TFV maintains
231 a constant value after 72 h both in POA and ambient PM.

232 COM can be decomposed and transformed due to photodegradation in aerosol (Wong et al.,
233 2015). Fluorophores are studied by the approach of EEMs-PARAFAC. Although previous study
234 has analyzed the water-soluble and methanol-soluble fluorophores separately (Tang et al., 2020a),
235 based on the Chen's studies (2020; 2016b), water-soluble and methanol-soluble samples were
236 combined to create the PARAFAC model to illustrate the distribution of fluorophores in WSOM
237 and MSOM and solvent had no significant effect on the EEMs of complex mixtures in aerosol. As
238 shown in **Figure 3(A)**, four fluorophores are identified. The fluorescence peaks of C1 and C2 appear
239 at (Ex./Em. = 224/434 nm) and (Ex./Em. = 245/402 nm). The peaks are similar to high and low
240 oxidation HULIS, respectively (Chen et al., 2016b; Birdwell and Engel, 2010). The peaks of C3 and
241 C4 appear at (Ex./Em. = 220/354 nm) and (Ex./Em. = 277/329 nm) and these two fluorophores are
242 associated with protein-like organic matter (PLOM-1 and PLOM-2) (Sierra et al., 2005; Huguet et
243 al., 2009; Chen et al., 2016a and 2016b; Coble, 2007; Fellman et al., 2009).

244 The content of fluorophores changes significantly during the photodegradation process. In
245 POA (**Figure 3(B)**), the relative content of high-oxidation HULIS (C1) increases by 63.0% and the
246 relative content of low oxidation HULIS (C2) decreases by 88.0% in WSOM. Changes in proportion
247 indicate that high-oxidation HULIS fluorophore (C1) could be generated and low oxidation HULIS
248 (C2) may be converted into high oxidation HULIS (C1) due to photooxidation (Tang et al., 2020b;
249 Chen et al., 2020). PLOM (C3&C4) decreases 19.7%, which indicates PLOM (C3&C4) can be
250 photodegraded. In MSOM of POA, no regularity of variation is found in low oxidation HULIS (C2)
251 and PLOM (C3&C4) and the content of high-oxidation HULIS (C1) increases by 17.5%, which can
252 be attributed to photo-mediated secondary reaction.

253 The contents of PLOM (C3&C4) in ambient PM (19.4%) (**Figure 3(C)**) are significantly lower
254 than that in POA (43.3%). The content of high-oxidation HULIS (C1) multiplied 6.9 times and the
255 low-oxidation HULIS (C2) decreases by 40.2% in WSOM, the variation is similar to POA. Thus,
256 high-oxidation HULIS could be used to trace the degree of aerosols photo-aging. In MSOM of

257 ambient PM, the content of high-oxidation HULIS (C1) increases by 43.5% and no regularity of
 258 variation is found in low oxidation HULIS (C2) and PLOM (C3&C4).

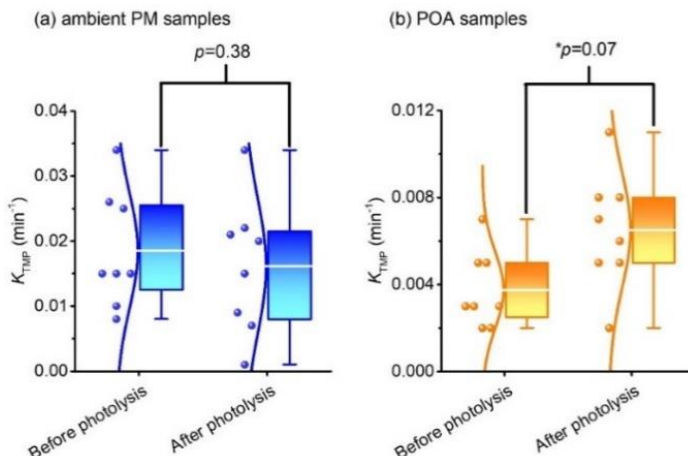


259
 260 **Figure 3** (A) EEM spectra of fluorophores; (B) Changes in proportion of fluorophores in POA;
 261 proportion of fluorophores in ambient PM. *: The data of 3-day photolysis of water-soluble fluorophores in winter
 262 is unavailable.

263 3.3 Effect of COM photodegradation on aerosol photochemical reactivity

264 COM photodegradation has a significant effect on photochemical reactivity of COM in aerosol.
 265 The photochemical activity is quantitative analyzed by the yield of ${}^3\text{COM}^*$ and ${}^1\text{O}_2$. Only WSOM
 266 of original and photolyzed samples was used to measure the yield of ${}^3\text{COM}^*$ (Original samples with
 267 photodegradation time of 0, photolyzed samples with photodegradation time of 7d; details of
 268 samples are described in section 2.2). **Figure 4** shows the variation of triplet state generation before
 269 and after the photodegradation (Consumption curves of TMP are shown in **Figure S8**). In ambient
 270 PM, compared with original samples, the generation rate of triplet state decreases by 11% on
 271 average in photolyzed samples, while statistical analysis shows that the changes are not obvious (p
 272 = 0.38, two-tailed test). On the contrary, in POA, photodegradation promotes triplet state generation
 273 significantly, the triplet state generation rate increases by 75% on average in photolyzed samples.
 274 (p = 0.07, two-tailed test). The results that triplet state generation remains unchanged or increases
 275 in different aerosols following photodegradation are unexpected and can be explained by recent
 276 study (Chen et al. 2021): on the one hand, only a small proportion of water-soluble OM could

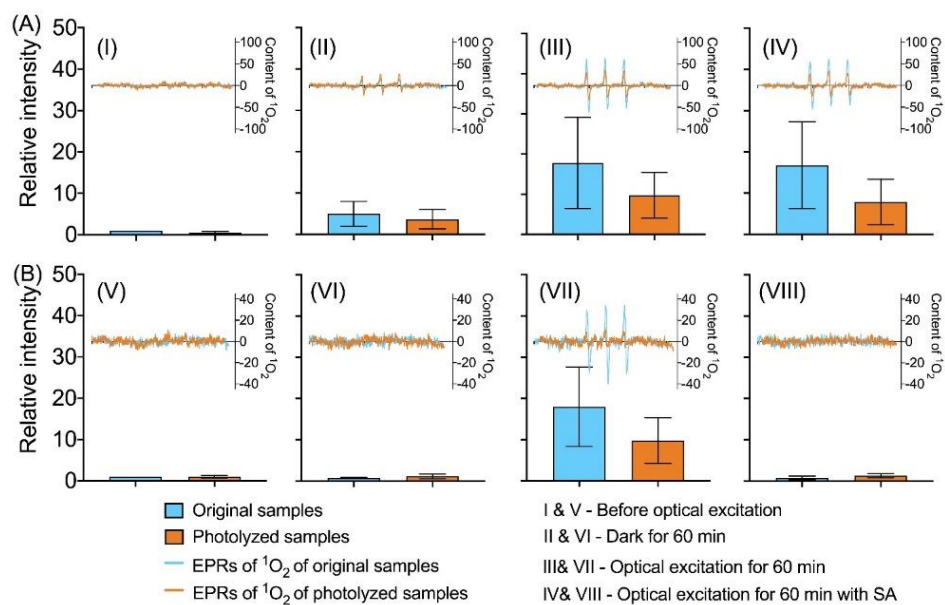
277 generate triplet state in aerosol and fluorophores do not represent the OM with the ability to generate
 278 triplet state. Therefore, triplet state generation could not be evaluated only by fluorescence intensity.
 279 On the other hand, we use a high concentration of TMP, in this case, TMP mainly captures high-
 280 energy triplet state (Rosado-Lausell et al., 2013; Chen et al., 2021). Thus, COM, that could generate
 281 a high-energy triplet state, may not be photodegraded in ambient PM.



282
 283 **Figure 4** Changes in the triplet state generation. (a) Ambient PM; (b) POA. The line from bottom to top in the box
 284 plots are minimum, first quartile, the average value (white lines), third quartile, and maximum, respectively. The p -
 285 value is the probability that two sets of data have the same level (two-tailed test). * represents a significant difference
 286 at the 0.1 level.

287 COM can generate triplet state and further generate singlet oxygen (McNeill and Canonica,
 288 2016). The effect of COM photodegradation on singlet oxygen is studied. WSOM of original and
 289 photolyzed samples was used to measure the yield of ${}^1\text{O}_2$ (EPR spectra of all samples is shown in
 290 **Figure S9** and **Figure S10**). As shown in **Figure 5**, a decrease in the yield of ${}^1\text{O}_2$ reveals the
 291 inhibiting effect of COM photodegradation on photochemical activity both in ambient PM and POA.
 292 In POA, as shown in **Figure 5(A)**, (I) Before optical excitation, there is little ${}^1\text{O}_2$ both in original
 293 and photolyzed samples; (II) After 60 min in dark, ${}^1\text{O}_2$ are generated both in original and photolyzed
 294 samples, which suggests POA could generate ${}^1\text{O}_2$ without optical excitation. The content of ${}^1\text{O}_2$ in
 295 original samples is higher than that in photolyzed samples; (III) After 60 minutes of optical
 296 excitation, as expected, compared with the samples without optical excitation, the content of ${}^1\text{O}_2$
 297 increases by 3 times both in original and photolyzed samples. The content of ${}^1\text{O}_2$ in original samples
 298 is also higher than that in photolyzed samples (42.1%), which prove the inhibiting effect of COM
 299 photodegradation on ${}^1\text{O}_2$ generation; (IV) However, the content of ${}^1\text{O}_2$ is nearly unchanged when
 300 the triplet state is quenched by sorbic acid. Therefore, the results indicate that the low-energy
 301 ${}^3\text{COM}^*$ ($E_T < 239$ kJ/mol) may be the main precursor for ${}^1\text{O}_2$ ($E_T = 94$ kJ/mol) in POA, because
 302 sorbic acid is a capturing agent for high-energy triplet state (triplet energies $E_T = 239\text{--}247$ kJ/mol)
 303 (Zhou et al., 2019; Moor et al., 2019). In addition, COM photodegradation does not change the
 304 mechanism of low-energy ${}^3\text{COM}^*$ generating ${}^1\text{O}_2$ in POA.

305 In ambient PM, as shown in **Figure 5(B)**, (V) Before optical excitation, the content of ${}^1\text{O}_2$ is
 306 very low in original and photolyzed samples, which is similar to POA; (VI) Compared with (V), the
 307 content of ${}^1\text{O}_2$ is almost unchanged after 60 min in dark, which is different from POA. The result
 308 suggests ambient PM could not generate ${}^1\text{O}_2$ without optical excitation. (VII) After 60 minutes of
 309 optical excitation, the content of ${}^1\text{O}_2$ increases significantly and the content of ${}^1\text{O}_2$ in original
 310 samples is higher than that in photolyzed samples (41.0% higher). (VIII) When the triplet state is
 311 quenched by sorbic acid, ${}^1\text{O}_2$ does not be generated. The result suggests that the precursor of ${}^1\text{O}_2$ is
 312 quenched and ${}^1\text{O}_2$ is mainly generated by high-energy ${}^3\text{COM}^*$ in ambient PM. COM with the ability
 313 of generating high-energy triplet state could be photodegraded, which directly leads to the decrease
 314 in ${}^1\text{O}_2$ in ambient PM. The quenching effects of sorbic acid on triplet state in POA and ambient PM
 315 are different because of the different energy of triplet state.



316
 317 **Figure 5** Changes in COM generating ${}^1\text{O}_2$ before and after photodegradation. (A) POA; (B) Ambient POA.

318 4. Implication

319 We made a comprehensive study in COM photodegradation and the effect of COM
 320 photodegradation on optical property, chemical component, and photochemical reactivity to reveal
 321 the characteristics of COM photodegradation. COM photodegradation could result in reduction of
 322 carbon content, attenuation of optical property, and change in fluorescent component. We also
 323 proposed that COM photodegradation should be evaluated from three aspects for further study. (1)
 324 The impact of COM photodegradation on carbon content was unclear. Previous studies have
 325 revealed that WSOC did not significantly change in the river DOM (Gonsior et al., 2009) and 0.2%
 326 of DOC was mineralized (Tranvik et al., 1998). However, the observation in the study suggested
 327 that changes in carbon content were different in aerosols, which could be attributed to the
 328 differences in original components. (2) Attenuation in optical properties was significant. Absorption
 329 coefficient and fluorescence intensity could be thought of as a tracer for molecular weight (Stewart

330 & Wetzel, 1980). Therefore, optical properties indicated the changes in molecular weight of COM
331 during the photodegradation process. The characteristic could be suitable for exploring the impact
332 of photodegradation on COM components. (3) COM Photodegradation may dominate the
333 fluorophores components (Aiona et al., 2018; Timko et al., 2015). High molecular weight COM
334 could be decomposed into low molecular weight COM during the photodegradation process. The
335 conversion of low-oxidation HULIS to high-oxidation HULIS was observed. Changes in COM may
336 represent the oxidation degree of organic substances. Therefore, we suggested that optical parameter
337 and oxidation degree of organic molecules should be used for characterizing the aerosol photo-aging
338 process (Maizel et al., 2017).

339 Photodegradation could not only change the properties and components of COM, but also
340 change their photochemical reactivity, which further had a potential impact on the aerosol fate.
341 Photodegradation and/or conversion of COM could be considered to be the main influence factor
342 for photochemical reaction capacity (McNight et al., 2001; Zepp et al., 1985). Photochemical
343 reactivity was quantified by the yield of triplet state and $^1\text{O}_2$ in our study. However, two different
344 methods, two different results. COM photodegradation could restrain $^1\text{O}_2$ generation but the effect
345 of photodegradation on $^3\text{COM}^*$ was unclear. Photodegradation had a significant inhibiting effect
346 on the $^1\text{O}_2$ yield in aerosols (Latch et al. 2006; Chen et al., 2018). We insisted that aerosol aging
347 would be changed by photodegradation due to the yield of $^1\text{O}_2$ was changed. Changes in triplet state
348 generation were uncertain in ambient PM and POA. There were two reasons for this. On the one
349 hand, only a small amount of COM was the precursor of $^3\text{COM}^*$ in aerosols. On the other hand, the
350 energy of capturing agents was closely related to $^3\text{COM}^*$ quantification and thereby $^3\text{COM}^*$ could
351 not be captured completely. Other capturing agents may lead to different results. Thus, $^3\text{COM}^*$
352 could not properly illustrate photodegradation. COM photodegradation could play an important role
353 in the content of ROS and ROS could calibrate the COM photooxidation (Claeys et al., 2004). Given
354 the results, the interaction effect was significant in aerosol.

355 In summary, atmospheric photochemistry process had a remarkable impact on aerosol aging.
356 Prediction of atmospheric lifetime and improvement of quality were strongly associated with
357 photochemistry. We proved that carbon content, absorption coefficient, fluorescence intensity, and
358 photochemical reactivity were useful to reflect COM photodegradation process and aerosol fate. In
359 addition, COM photodegradation had a different impact on chemical reactivity in different aerosols,
360 which may have different mechanisms. Therefore, the mechanisms of COM photodegradation
361 affecting aerosol photo-aging deserved further investigation.

362 **Data availability.** All data that support the findings of this study are available in this article and its
363 Supplement or from the corresponding author on request.

364 **Supporting information.** Additional details, including Tables S1–S5, Figures S1–S10, calculation
365 of optical characteristics of WSOM/WISOM, are contained in the SI.

366 **Author contributions.** QC and ZM designed the experiments and data analysis. ZM and LZ
367 performed sample collection. ZM performed the photochemical experiment. ZM and DG performed
368 the OC/EC analysis and optical analysis. HL performed the EPR analysis. QC prepared the paper
369 with the contributions from all co-authors.

370 **Competing interests.** The authors declare that they have no conflict of interest.

371 **Acknowledgments.** We thank the National Natural Resources Foundation for its financial support.

372 **Financial support.** This work was supported by the National Natural Science Foundation of China
373 (grant numbers 41877354 and 41703102), and the Youth Science and Technology Nova Program
374 of Shaanxi Province (2021KJXX-36).

375 **References**

376 Aiona, P. K., Luek, J. L., Timko, S. A., Powers, L. C., Gonsior, M., and Nizkorodov, S. A.: Effect of Photolysis on
377 Absorption and Fluorescence Spectra of Light-Absorbing Secondary Organic Aerosols, *ACS Earth Space
378 Chem.*, 2, 235-245, 10.1021/acsearthspacechem.7b00153, 2018.

379 Altieri, K. E., Carlton, A. G., Lim, H. J., Turpin, B. J., and Seitzinger, S. P.: Evidence for oligomer formation in
380 clouds: Reactions of isoprene oxidation products, *Environ. Sci. Technol.*, 40, 4956-4960,
381 <http://dx.doi.org/10.1021/es052170n>, 2006.

382 Altieri, K. E., Seitzinger, S. P., Carlton, A. G., Turpin, B. J., Klein, G. C., and Marshall, A. G.: Oligomers formed
383 through in-cloud methylglyoxal reactions: Chemical composition, properties, and mechanisms investigated by
384 ultra-high resolution FT-ICR mass spectrometry, *Atmos. Environ.*, 42, 1476-1490,
385 <http://dx.doi.org/10.1016/j.atmosenv.2007.11.015>, 2008.

386 Andreae, M. O., and Gelencser, A.: Black carbon or brown carbon? The nature of light-absorbing carbonaceous
387 aerosols, *Atmos. Chem. Phys.*, 6, 3131-3148, <http://dx.doi.org/10.5194/acp-6-3131-2006>, 2006.

388 Atkinson, R.; Baulch, D. L.; Cox, R. A.; Crowley, J. N.; Hampson, R. F.; Hynes, R. G.; Jenkin, M. E.; Rossi, M. J.;
389 Troe, J.: Evaluated kinetic and photochemical data for atmospheric chemistry: Volume II - gas phase reactions
390 of organic species, *Atmos. Chem. Phys.*, 6, 3625-4055, <http://dx.doi.org/10.5194/acp-6-3625-2006>, 2006.

391 Birdwell, J. E., and Engel, A. S.: Characterization of dissolved organic matter in cave and spring waters using
392 UV-Vis absorbance and fluorescence spectroscopy, *Org. Geochem.*, 41,
393 <http://dx.doi.org/10.1016/j.orggeochem.2009.11.002>, 2010.

394 Budisulistiorini, S. H.; Riva, M.; Williams, M.; Chen, J.; Itoh, M.; Surratt, J. D.; Kuwata, M.: Light-Absorbing
395 Brown Carbon Aerosol Constituents from Combustion of Indonesian Peat and Biomass. *Environ. Sci. Technol.*,
396 51, 4415-4423, <http://dx.doi.org/10.1021/acs.est.7b00397>, 2017.

397 Canonica, S.; Hellrung, B.; Müller, P.; Wirz, J.: Aqueous Oxidation of Phenylurea Herbicides by Triplet Aromatic
398 Ketones, *Environ. Sci. Tech.*, 40, 6636-6641, <https://doi.org/10.1021/es0611238>, 2006.

399 Carlton, A. G.; Turpin, B. J.; Altieri, K. E.; Seitzinger, S.; Reff, A.; Lim, H. J.; Ervens, B.: Atmospheric oxalic acid
400 and SOA production from glyoxal: Results of aqueous photooxidation experiments, *Atmos. Environ.*, 41, 7588-
401 7602, <http://dx.doi.org/10.1016/j.atmosenv.2007.05.035>, 2007.

402 Chen, Q., Miyazaki, Y., Kawamura, K., Matsumoto, K., Coburn, S., Volkamer, R., Iwamoto, Y., Kagami, S., Deng,
403 Y., Ogawa, S., Ramasamy, S., Kato, S., Ida, A., Kajii, Y., and Mochida, M.: Characterization of Chromophoric

404 Water-Soluble Organic Matter in Urban, Forest, and Marine Aerosols by HR-ToF-AMS Analysis and
405 Excitation-Emission Matrix Spectroscopy, Environ. Sci. Technol., 50, 10351-10360,
406 <http://dx.doi.org/10.1021/acs.est.6b01643>, 2016a.

407 Chen, Q. C., Ikemori, F., and Mochida, M.: Light Absorption and Excitation-Emission Fluorescence of Urban
408 Organic Aerosol Components and Their Relationship to Chemical Structure, Environ. Sci. Technol., 50, 10859-
409 10868, <http://dx.doi.org/10.1021/acs.est.6b02541>, 2016b.

410 Chen, Q., Li, J., Hua, X., Jiang, X., Mu, Z., Wang, M., Wang, J., Shan, M., Yang, X., Fan, X., Song, J., Wang, Y.,
411 Guan, D., and Du, L.: Identification of species and sources of atmospheric chromophores by fluorescence
412 excitation-emission matrix with parallel factor analysis, Sci. Total Environ., 718, 137322,
413 <http://dx.doi.org/10.1016/j.scitotenv.2020.137322>, 2020.

414 Chen, Q.; Mu, Z.; Xu, L.; Wang, M.; Wang, J.; Shan, M.; Fan, X.; Song, J.; Wang, Y.; Lin, P.; Du, L.: Triplet-state
415 organic matter in atmospheric aerosols: Formation characteristics and potential effects on aerosol aging, Atmos.
416 Environ., 252, 118343, <https://doi.org/10.1016/j.atmosenv.2021.118343>, 2021.

417 Chen, Y., Zhang, X., and Feng, S.: Contribution of the Excited Triplet State of Humic Acid and Superoxide Radical
418 Anion to Generation and Elimination of Phenoxy Radical, Environ. Sci. Technol., 52, 8283-8291,
419 <http://dx.doi.org/10.1021/acs.est.8b00890>, 2018.

420 Cheng, Y., He, K. B., Du, Z. Y., Engling, G., Liu, J. M., Ma, Y. L., Zheng, M., and Weber, R. J.: The characteristics
421 of brown carbon aerosol during winter in Beijing, Atmos. Environ., 127, 355-364,
422 <http://dx.doi.org/10.1016/j.atmosenv.2015.12.035>, 2016.

423 Claeys, M.; Graham, B.; Vas, G.; Wang, W.; Vermeylen, R.; Pashynska, V.; Cafmeyer, J.; Guyon, P.; Andreae, M.
424 O.; Artaxo, P.; Maenhaut, W.: Formation of secondary organic aerosols through photooxidation of isoprene,
425 Science, 303, 1173-1176, <http://dx.doi.org/10.1126/science.1092805>, 2004.

426 Coble, P. G.: Marine optical biogeochemistry: the chemistry of ocean color, Chem. Rev., 107, 402-418,
427 <http://dx.doi.org/10.1021/cr050350+>, 2007.

428 Duarte, R. M. B. O., Pio, C. A., and Duarte, A. C.: Spectroscopic study of the water-soluble organic matter isolated
429 from atmospheric aerosols collected under different atmospheric conditions, Anal. Chim. Acta, 530, 7-14,
430 <http://dx.doi.org/10.1016/j.aca.2004.08.049>, 2005.

431 Encinas, M. V.; Lissi, E. A.; Olea, A. F.: Quenching of triplet benzophenone by vitamins E and C and by sulfur
432 containing amino acids and peptides, Photochem. Photobiol., 42, 347-52, [http://dx.doi.org/10.1111/j.1751-1097.1985.tb01580.x](http://dx.doi.org/10.1111/j.1751-
433 1097.1985.tb01580.x), 1985.

434 Fellman, J. B., Miller, M. P., Cory, R. M., D'Amore, D. V., and White, D.: Characterizing Dissolved Organic Matter
435 Using PARAFAC Modeling of Fluorescence Spectroscopy: A Comparison of Two Models, Environ. Sci.
436 Technol., 43, 6228-6234, <http://dx.doi.org/10.1021/es900143g>, 2009.

437 George, C.; Ammann, M.; D'Anna, B.; Donaldson, D. J.; Nizkorodov, S. A.: Heterogeneous Photochemistry in the
438 Atmosphere. Chem. Rev., 115, 4218-4258, [10.1021/cr500648z](https://doi.org/10.1021/cr500648z), 2015.

439 Gonsior, M., Peake, B. M., Cooper, W. T., Podgorski, D., D'Andrilli, J., and Cooper, W. J.: Photochemically induced
440 changes in dissolved organic matter identified by ultrahigh resolution fourier transform ion cyclotron resonance
441 mass spectrometry, Environ. Sci. Technol., 43, 698-703, <http://dx.doi.org/10.1021/es8022804>, 2009.

442 Gruber, E. R., and Rudich, Y.: Atmospheric HULIS: how humic-like are they? A comprehensive and critical review,
443 Atmos. Chem. Phys., 6, 729-753, <http://dx.doi.org/10.5194/acp-6-729-2006>, 2005.

444 Grieshop, A. P., Donahue, N. M., and Robinson, A. L.: Laboratory investigation of photochemical oxidation of
445 organic aerosol from wood fires 2: analysis of aerosol mass spectrometer data, Atmos. Chem. Phys., 9, 2227-
446 2240, <http://dx.doi.org/DOI 10.5194/acp-9-2227-2009>, 2009.

447 Haag, W. R., and Gassman, E.: Singlet oxygen in surface waters-Part II: Quantum yields of its production by some
448 natural humic materials as a function of wavelength, *Chemosphere*, 13, 641-650,
449 [http://dx.doi.org/10.1016/0045-6535\(84\)90200-5](http://dx.doi.org/10.1016/0045-6535(84)90200-5), 1984.

450 Harrison, A.W., Waterson, A.M., De Bruyn, W.J.: Spectroscopic and Photochemical Properties of Secondary Brown
451 Carbon from Aqueous Reactions of Methylglyoxal, *ACS Earth Space Chem.*, 4, 762-773,
452 <http://dx.doi.org/10.1021/acsearthspacechem.0c00061>, 2020.

453 Haynes, J. P., Miller, K. E., and Majestic, B. J.: Investigation into Photoinduced Auto-Oxidation of Polycyclic
454 Aromatic Hydrocarbons Resulting in Brown Carbon Production, *Environ. Sci. Technol.*, 53, 682-691,
455 <http://dx.doi.org/10.1021/acs.est.8b05704>, 2019.

456 Holmes, B. J., and Petrucci, G. A.: Water-soluble oligomer formation from acid-catalyzed reactions of levoglucosan
457 in proxies of atmospheric aqueous aerosols, *Environ. Sci. Technol.*, 40, 4983-4989,
458 <http://dx.doi.org/10.1021/es060646c>, 2006.

459 Huguet, A., Vacher, L., Relexans, S., Saubusse, S., Froidefond, J. M., and Parlanti, E.: Properties of fluorescent
460 dissolved organic matter in the Gironde Estuary, *Org. Geochem.*, 40,
461 <http://dx.doi.org/10.1016/j.orggeochem.2009.03.002>, 2009.

462 Jo, D. S.; Park, R. J.; Lee, S.; Kim, S. W.; Zhang, X.: A global simulation of brown carbon: implications for
463 photochemistry and direct radiative effect, *Atmos. Chem. Phys.*, 16, 3413-3432, <http://dx.doi.org/10.5194/acp-16-3413-2016>, 2016.

465 Karanasiou, A., Minguillón, M. C., Viana, M., Alastuey, A., Putaud, J.-P., Maenhaut, W., Panteliadis, P., Močnik,
466 G., Favez, O., and Kuhlbusch, T. A. J.: Thermal-optical analysis for the measurement of elemental carbon (EC)
467 and organic carbon (OC) in ambient air a literature review, *Atmos. Meas. Tech. Discuss.*, 8, 9649-9712,
468 <http://dx.doi.org/10.5194/amtd-8-9649-2015>, 2015.

469 Kaur, R., and Anastasio, C.: First Measurements of Organic Triplet Excited States in Atmospheric Waters, *Environ.*
470 *Sci. Technol.*, 52, 5218-5226, <http://dx.doi.org/10.1021/acs.est.7b06699>, 2018.

471 Latch, D. E., and McNeill, K.: Microheterogeneity of singlet oxygen distributions in irradiated humic acid solutions,
472 *Science*, 311, 1743-1747, <http://dx.doi.org/10.1126/science.1121636>, 2006.

473 Lee, H. J., Laskin, A., Laskin, J., and Nizkorodov, S. A.: Excitation-emission spectra and fluorescence quantum
474 yields for fresh and aged biogenic secondary organic aerosols, *Environ. Sci. Technol.*, 47, 5763-5770,
475 <http://dx.doi.org/10.1021/es400644c>, 2013.

476 Lee, H. J., Aiona, P. K., Laskin, A., Laskin, J., and Nizkorodov, S. A.: Effect of solar radiation on the optical
477 properties and molecular composition of laboratory proxies of atmospheric brown carbon, *Environ. Sci.*
478 *Technol.*, 48, 10217-10226, <http://dx.doi.org/10.1021/es502515r>, 2014.

479 Liu, J. M., Lin, P., Laskin, A., Laskin, J., Kathmann, S. M., Wise, M., Taylor, R., Imholt, F., Selimovic, V., and
480 Shilling, J. E.: Optical properties and aging of light-absorbing secondary organic aerosol, *Atmos. Chem. Phys.*,
481 16, 12815-12827, <http://dx.doi.org/10.5194/acp-16-12815-2016>, 2016.

482 Maizel, A. C., Li, J., and Remucal, C. K.: Relationships Between Dissolved Organic Matter Composition and
483 Photochemistry in Lakes of Diverse Trophic Status, *Environ. Sci. Technol.*, 51, 9624-9632,
484 <http://dx.doi.org/10.1021/acs.est.7b01270>, 2017.

485 Mang, S. A.; Henricksen, D. K.; Bateman, A. P.; Andersen, M. P. S.; Blake, D. R.; Nizkorodov, S. A.: Contribution
486 of Carbonyl Photochemistry to Aging of Atmospheric Secondary Organic Aerosol, *J. Phys. Chem. A*, 112,
487 8337-8344, <http://dx.doi.org/10.1021/jp804376c>, 2008.

488 Marciniak, B.; Bobrowski, K.; Hug, G. L.: Quenching of triplet states of aromatic ketones by sulfur-containing
489 amino acids in solution. Evidence for electron transfer, *J. Phys. Chem.*, 97, 11937-11943, 10.1021/j100148a015,
490 1993.

491 McKnight, D. M., Boyer, E. W., Westerhoff, P. K., Doran, P. T., Kulbe, T., and Andersen, D. T.: Spectrofluorometric
492 characterization of dissolved organic matter for indication of precursor organic material and aromaticity,
493 Limnol. Oceanogr., 46, 38-48, <http://dx.doi.org/10.4319/lo.2001.46.1.0038>, 2001.

494 McNeill, K., and Canonica, S.: Triplet state dissolved organic matter in aquatic photochemistry: reaction
495 mechanisms, substrate scope, and photophysical properties, Environ. Sci. Process Impacts, 18, 1381-1399,
496 <http://dx.doi.org/10.1039/c6em00408c>, 2016.

497 Moor, K. J., Schmitt, M., Erickson, P. R., and McNeill, K.: Sorbic Acid as a Triplet Probe: Triplet Energy and
498 Reactivity with Triplet-State Dissolved Organic Matter via $^1\text{O}_2$ Phosphorescence, Environ. Sci. Technol.,
499 <http://dx.doi.org/10.1021/acs.est.9b01787>, 2019.

500 Mu, Z., Chen, Q. C., Wang, Y. Q., Shen, Z. X., Hua, X. Y., Zhang, Z. M., Sun, H. Y., Wang, M. M., and Zhang, L.
501 X.: Characteristics of Carbonaceous Aerosol Pollution in PM2.5 in Xi'an, Huan Jing Ke Xue, 40, 1529-1536,
502 <http://dx.doi.org/10.13227/j.hjx.201807135>, 2019.

503 Murphy, K. R., Stedmon, C. A., Graeber, D., and Bro, R.: Fluorescence spectroscopy and multi-way techniques.
504 PARAFAC, Anal. Methods, 5, 6557-6566, <http://dx.doi.org/10.1039/c3ay41160e>, 2013.

505 Nebbioso, A.; Piccolo, A.: Molecular characterization of dissolved organic matter (DOM): a critical review, Anal.
506 Bioanal., Chem. 405, 109-124, <http://dx.doi.org/10.1007/s00216-012-6363-2>, 2013.

507 Paul Hansard, S., Vermilyea, A. W., and Voelker, B. M.: Measurements of superoxide radical concentration and
508 decay kinetics in the Gulf of Alaska, Deep Sea Res., Part I, 57, 1111-1119,
509 <http://dx.doi.org/10.1016/j.dsr.2010.05.007>, 2010.

510 Perri, M. J., Seitzinger, S., and Turpin, B. J.: Secondary organic aerosol production from aqueous photooxidation of
511 glycolaldehyde: Laboratory experiments, Atmos. Environ., 43, 1487-1497,
512 <http://dx.doi.org/10.1016/j.atmosenv.2008.11.037>, 2009.

513 Richards-Henderson, N. K., Pham, A. T., Kirk, B. B., and Anastasio, C.: Secondary organic aerosol from aqueous
514 reactions of green leaf volatiles with organic triplet excited states and singlet molecular oxygen, Environ. Sci.
515 Technol., 49, 268-276, <http://dx.doi.org/10.1021/es503656m>, 2015.

516 Rosado-Lausell, S.L., Wang, H.T., Gutierrez, L., Romero-Maraccini, O.C., Niu, X.Z., Gin, K.Y.H., Croue, J.P.,
517 Nguyen, T.H.: Roles of singlet oxygen and triplet excited state of dissolved organic matter formed by different
518 organic in bacteriophage MS2 inactivation, Water Res., 47, 4869-4879,
519 <http://dx.doi.org/10.1016/j.watres.2013.05.018>, 2013.

520 Rosario-Ortiz, F. L., and Canonica, S.: Probe Compounds to Assess the Photochemical Activity of Dissolved
521 Organic Matter, Environ. Sci. Technol., 50, 12532-12547, <http://dx.doi.org/10.1021/acs.est.6b02776>, 2016.

522 Saleh, R., Hennigan, C. J., McMeeking, G. R., Chuang, W. K., Robinson, E. S., Coe, H., Donahue, N. M., and
523 Robinson, A. L.: Absorptivity of brown carbon in fresh and photo-chemically aged biomass-burning emissions,
524 Atmos. Chem. Phys., 13, 7683-7693, <http://dx.doi.org/10.5194/acp-13-7683-2013>, 2013.

525 Sharpless, C. M.: Lifetimes of Triplet Dissolved Natural Organic Matter (DOM) and the Effect of NaBH_4 Reduction
526 on Singlet Oxygen Quantum Yields: Implications for DOM Photophysics, Environ. Sci. Technol., 46, 4466-
527 4473, <http://dx.doi.org/10.1021/es300217h>, 2012.

528 Sierra, M. M. D., Giovanelia, M., Parlanti, E., and Soriano-Sierra, E. J.: Fluorescence fingerprint of fulvic and humic
529 acids from varied origins as viewed by single-scan and excitation/emission matrix techniques, Chemosphere,
530 58, <http://dx.doi.org/10.1016/j.chemosphere.2004.09.038>, 2005.

531 Stewart, A. J.; Wetzel, R. G: Fluorescence: absorbance ratios—a molecular-weight tracer of dissolved organic matter,
532 Limnol. Oceanogr., 25, 559-564, <https://doi.org/10.4319/lo.1980.25.3.0559>, 1980.

533 Szymczak, R., and Waite, T.: Generation and decay of hydrogen peroxide in estuarine waters, Mar. Freshwater Res.,
534 39, 289-299, <http://dx.doi.org/10.1071/MF9880289>, 1988.

535 Tang, J., Li, J., Su, T., Han, Y., Mo, Y.Z., Jiang, H.X., Cui, M., Jiang, B., Chen, Y.J., Tang, J.H., Song, J.Z., Peng,
536 P.A., Zhang, G.: Molecular compositions and optical properties of dissolved brown carbon in biomass burning,
537 coal combustion, and vehicle emission aerosols illuminated by excitation-emission matrix spectroscopy and
538 Fourier transform ion cyclotron resonance mass spectrometry analysis. *Atmos. Chem. Phys.* 20, 2513-2532,
539 <http://dx.doi.org/10.5194/acp-20-2513-2020>, 2020a.

540 Tang, S. S., Li, F. H., Tsona, N. T., Lu, C. Y., Wang, X. F., and Du, L.: Aqueous-Phase Photooxidation of Vanillic
541 Acid: A Potential Source of Humic-Like Substances (HULIS), *Acs Earth and Space Chem.*, 4, 862-872,
542 <http://dx.doi.org/10.1021/acsearthspacechem.0c00070>, 2020b.

543 Timko, S.; Maydanov, A.; Pittelli, S.; Conte, M.; Cooper, W.; Koch, B.; Schmitt-Kopplin, P.; Gonsior, M.: Depth-
544 dependent photodegradation of marine dissolved organic matter, *Front. Mar. Sci.*, 2,
545 <https://doi.org/10.3389/fmars.2015.00066>, 2015.

546 Tranvik, L.; Kokalj, S.: Decreased biodegradability of algal DOC due to interactive effects of UV radiation and
547 humic matter, *Aquat. Microb. Ecol.*, 14, 301-307, <https://doi.org/10.3354/ame014301>, 1998.

548 Wawzonek, S.; Laitinen, H. A.: The Reduction of Unsaturated Hydrocarbons at the Dropping Mercury Electrode.
549 II. Aromatic Polynuclear Hydrocarbons, *J. Am. Chem. Soc.*, 64, 2365-2368,
550 <http://dx.doi.org/10.1021/ja01262a040>, 1942.

551 Wenk, J., Aeschbacher, M., Salhi, E., Canonica, S., von Gunten, U., and Sander, M.: Chemical oxidation of dissolved
552 organic matter by chlorine dioxide, chlorine, and ozone: effects on its optical and antioxidant properties,
553 *Environ. Sci. Technol.*, 47, 11147-11156, <http://dx.doi.org/10.1021/es402516b>, 2013.

554 Wong, J. P. S., Zhou, S. M., and Abbatt, J. P. D.: Changes in Secondary Organic Aerosol Composition and Mass
555 due to Photolysis: Relative Humidity Dependence, *J. Phys. Chem. A*, 119, 4309-4316,
556 <http://dx.doi.org/10.1021/jp506898c>, 2015.

557 Xu, W.; Gao, Q.; He, C.; Shi, Q.; Hou, Z.-Q.; Zhao, H.-Z.: Using ESI FT-ICR MS to Characterize Dissolved Organic
558 Matter in Salt Lakes with Different Salinity, *Environ. Sci. Technol.*, 54, 12929-12937,
559 <http://dx.doi.org/10.1021/acs.est.0c01681>, 2020.

560 Yang, X. M.; Yuan, J.; Yue, F. J.; Li, S. L.; Wang, B. L.; Mohinuzzaman, M.; Liu, Y. J.; Senesi, N.; Lao, X. Y.; Li,
561 L. L.; Liu, C. Q.; Ellam, R. M.; Vione, D.; Mostofa, K. M. G.: New insights into mechanisms of sunlight- and
562 dark-mediated high-temperature accelerated diurnal production-degradation of fluorescent DOM in lake waters,
563 *Sci. Total Environ.*, 760, 14, <http://dx.doi.org/10.1016/j.scitotenv.2020.143377>, 2021.

564 Zappoli, S., Andracchio, A., Fuzzi, S., Facchini, M. C., Gelencser, A., Kiss, G., Krivacsy, Z., Molnar, A., Meszaros,
565 E., Hansson, H. C., Rosman, K., and Zebuhr, Y.: Inorganic, organic and macromolecular components of fine
566 aerosol in different areas of Europe in relation to their water solubility, *Atmos. Environ.*, 33, 2733-2743,
567 [http://dx.doi.org/10.1016/S1352-2310\(98\)00362-8](http://dx.doi.org/10.1016/S1352-2310(98)00362-8), 1999.

568 Zepp, R. G., Schlotzhauer, P. F., and Sink, R. M.: Photosensitized transformations involving electronic energy
569 transfer in natural waters: role of humic substances, *Environ. Sci. Technol.*, 19, 74-81,
570 <http://dx.doi.org/10.1021/es00131a008>, 1985.

571 Zhang, D., Yan, S., and Song, W.: Photochemically induced formation of reactive oxygen species (ROS) from
572 effluent organic matter, *Environ. Sci. Technol.*, 48, 12645-12653, <http://dx.doi.org/10.1021/es5028663>, 2014.

573 Zhao, R., Lee, A. K. Y., Huang, L., Li, X., Yang, F., and Abbatt, J. P. D.: Photochemical processing of aqueous
574 atmospheric brown carbon, *Atmos. Chem. Phys.*, 15, 6087-6100, <http://dx.doi.org/10.5194/acp-15-6087-2015>,
575 2015.

576 Zhao, Y.; Hallar, A. G.; Mazzoleni, L. R: Atmospheric organic matter in clouds: exact masses and molecular formula
577 identification using ultrahigh-resolution FT-ICR mass spectrometry, *Atmos. Chem. Phys.*, 13, 12343-12362.
578 <http://dx.doi.org/10.5194/acp-13-12343-2013>, 2013.

579 Zhong, M., and Jang, M.: Dynamic light absorption of biomass-burning organic carbon photochemically aged under
580 natural sunlight, *Atmos. Chem. Phys.*, 14, 1517-1525, <http://dx.doi.org/10.5194/acp-14-1517-2014>, 2014.

581 Zhou, H., Yan, S., Lian, L., and Song, W.: Triplet-State Photochemistry of Dissolved Organic Matter: Triplet-State
582 Energy Distribution and Surface Electric Charge Conditions, *Environ. Sci. Technol.*, 53, 2482-2490,
583 <http://dx.doi.org/10.1021/acs.est.8b06574>, 2019.